Electron collisions with small esters: a joint experimental-theoretical investigation

G. L. C. de Souza,[1] L. A. da Silva,[2] W. J. C. de Sousa,[3] R. T. Sugohara,[4] I. Iga,[2] A. S. dos Santos,[5] L. E. Machado,[5] M. G. P. Homem,[2] L. M. Brescansin,[6] R. R. Lucchese,[7] and M.-T. Lee[2]

[1]*Departamento de Química, UFMT, 78060-900 Cuiabá, MT, Brazil*

[2]*Departamento de Química, UFSCar, 13565-905 São Carlos, SP, Brazil*

[3]*Instituto de Ciências Exatas e Tecnologia, UFAM, 69100-000 Itacoatiara, AM, Brazil*

[4]*IFSP - Campus Itapetininga, 18202-000 Itapetininga, SP, Brazil*

[5]*Departamento de Física, UFSCar, 13565-905 São Carlos, SP, Brazil*

[6]*Instituto de Física "Gleb Wataghin", UNICAMP, 13083-970 Campinas, SP, Brazil*

[7]*Chemistry Department, Texas A&M University, College Station, Texas 77842-3012, USA*

(Dated: February 10, 2016)

Abstract

A theoretical and experimental investigation on elastic electron scattering by two small esters, namely methyl formate and ethyl acetate, is reported. Experimental differential, integral, and momentum-transfer cross sections are given in the 30–1000 eV and 10°–120° ranges. The relative-flow technique was used to determine such quantities. Particularly for methyl formate, a theoretical study was also carried out in the 1–500 eV range. A complex optical potential derived from a Hartree-Fock molecular wave function was used to represent the collision dynamics, whereas the Padé approximation was used to solve the scattering equations. In addition, calculations based on the framework of the independent atom model (IAM) were also performed for both targets. In general, there is a good agreement between our experimental data and the present theoretical results calculated using the Padé approximation. The theoretical results using the IAM also agree well with the experimental data at 200 eV and above. Moreover, for methyl formate, our calculations have revealed a $^2A''$ (π^*) resonance at about 3.0 eV and a σ^* type resonance centered at about 8.0 eV in the $^2A'$ scattering channel. The π^* resonance is also seen in other targets containing a carbonyl group.

PACS numbers: 34.80.Bm

I. INTRODUCTION

The search for renewable energy sources is certainly strategic for all countries in order to controle global warming effects. In this regard, the use of biodiesel replacing fossil fuels is an important step. Chemically, biodiesels are mixtures of esters with long carbon chains which can be obtained from vegetable oils or animal fats via transesterification reactions [1]. Therefore, the investigation on electron interaction with small esters such as methyl formate and ethyl acetate may help the understanding of combustion of biodiesels. Besides, small esters were also observed in interstellar clouds. For instance, methyl formate together with its isomers, acetic acid and glycolaldehyde, were detected in hot molecular cores [2]. Moreover, this ester is much more abundant than its isomers with the ratio of 1864:103:1 relative to the acetic acid and glycolaldehyde, respectively [3]. Thus, cross sections for electron scattering by these species are important for the understanding of physical and chemical processes in that media [2].

Despite that, there is a lack of investigations on electron interaction with small esters in the literature. The electron diffraction method was applied to determine the molecular structure of methyl formate in 1980 [4]. Also, oscillator strengths for C1s and O1s in methyl formate were measured by Ishii and Hitchcock in 1988 [5] using an electron energy-loss spectroscopy technique. In addition, total ionization cross sections (TICS) for electron collisions with methyl formate and ethyl acetate were measured by Hudson *et al.* [6] at energies from near threshold to 285 eV. To our knowledge, there are neither other experimental nor theoretical studies on electron collisions with esters.

In the present study, we report a joint experimental-theoretical study of electron collisions with two small esters. More specifically, experimental differential (DCS), integral (ICS), and momentum-transfer (MTCS) cross sections for elastic electron scattering by methyl formate and ethyl acetate in the 30–1000 eV energy range are reported. The DCS were determined using the relative-flow technique (RFT), whereas experimental ICS and MTCS were generated from the measured DCS via a numerical integration procedure. Theoretically, the DCS, ICS, MTCS, as well as the grand-total (TCS) and total absorption (TACS) cross sections for e^-–methyl formate collisions were calculated using a combination of the molecular complex optical potential (MCOP) and the Padé approximation. These quantities are reported in the 1–500 eV energy range.

The organization of this work is as follows: In Sec. II, we present briefly the experimental procedure. In Sec. III, the used MCOP theory and details of the calculations are presented. In Sec. IV, we compare our calculated and measured data for methyl formate, whereas our experimental data for ethyl acetate are compared with the results calculated using the independent-atom model (IAM). Finally, in Sec. V, we present some conclusions.

II. EXPERIMENTAL

Methyl formate with purity better than 95% and ethyl acetate, better than 99%, used in the present experiment, were purchased from EMD Millipore and Synth, respectively. Details of our experimental setup and procedures were already presented in our previous works [7–14] and therefore will only be outlined here. Elastically scattered electron angular distributions were measured in the 30–1000 eV range using a crossed electron beam-molecular beam geometry. In our experiments, electronically inelastic scattered electrons were discriminated by using a retarding-field energy analyzer with resolution around 1.5 eV. This resolution does not allow the separation of the vibrationally elastic and inelastic processes, thus the measured intensities are vibrationally summed. Furthermore, the elastically scattered intensities were converted to absolute DCS using the RFT [15]. For that, Ar and N_2 were used as secondary standards. The details for the precise determination of the relative flows for the targets of interest and the secondary standards were also given in our previous work [10]. Moreover, the absolute DCS of Ar and N_2 available in the literature [16–18] in the 30–1000 eV range, were used to normalize our data. In principle, the intensities of scattered electrons for secondary standards and targets of interest for a given angle, should be measured using the ratio of pressures that ensures the equal mean-free-path condition. Nevertheless, as shown in one of our previous works [9], if the scattering intensities are obtained in a pressure region where they are proportional to the gaseous beam flux, the conversion of scattering intensity to DCS can be made regardless of the ratio of pressures. Such condition is satisfied in this work.

The estimation of uncertainties of the present data were carried out combining the experimental errors of both systematic and random natures [9, 14] with the quoted uncertainties for the secondary standards [16–18]. The overall estimated uncertainties are 16.5% at 30 eV, 21% at 50 eV, 15% at 800 and 1000 eV, and 11% at other energies.

The ICS and MTCS were obtained via a numerical integration over the DCS. An extrapolation procedure was used to estimate the DCS at scattering angles not covered experimentally. The trend of the theoretical results was followed in this procedure in order to reduce the arbitrariness. The overall uncertainties on ICS and MTCS were estimated to be 30% at 30 and 50 eV, and 25% at other energies.

III. THEORY AND NUMERICAL PROCEDURE

The theory used in this work was already presented in several of our previous articles [14, 19–21]. Basically, a molecular complex optical potential composed of static (U_{st}), exchange (U_{ex}), correlation-polarization (U_{cp}), and absorption (U_{ab}) contributions was used to represent the electron-target interaction. Further, the scattering equations with the MCOP were solved using the Padé approximation [22] which provides the body-frame transition T matrices. Such T matrices were transformed to laboratory-frame scattering amplitudes via an usual frame transformation [23].

In the present work, U_{st} and U_{ex} were derived exactly from the target wave function, whereas U_{cp} was obtained in the framework of the free-electron-gas model, derived from a parameter-free local density, as prescribed by Padial and Norcross [24]. Our calculated polarizabilities were used to generate the asymptotic form of U_{cp}.

The absorption potential U_{ab} was generated using the scaled quasi-free scattering model (SQFSM) of Lee *et al.* [25, 26] which is an improvement of the version 3 of the model absorption potential originally proposed by Staszewska *et al.* [27]. The Hara free-electron-gas-exchange potential [28] was used to generate the local exchange potential U_{ex}^{loc}.

The ground-state HF-SCF wave function of methyl formate was obtained using the triple-zeta valence (TZV-1d) basis set of GAMESS package [29]. At the experimental molecular geometry [30], this basis provided a total energy of -227.862862 hartrees, to be compared with the value of -229.157276 hartrees obtained by using the density functional theory (DFT) [30]. Our calculated electric dipole moment was 2.084 D, in fairly good agreement with the experimental value of 1.77 D [30]. The dipole polarizabilities calculated at the HF-SCF level using the same basis set were: $\alpha_{xx} = 28.85$ a.u., $\alpha_{yy} = 27.15$ a.u., and $\alpha_{zz} = 18.64$ a.u., resulting in an average dipole polarizability of $\alpha_0 = 24.88$ a.u., in good agreement with the theoretical value of 26.93 a.u. from the same DFT calculation [30].

In our calculations, the wave functions and interaction potentials, as well as the related matrices, were single-center expanded about the center-of-mass of the molecule in terms of the symmetry-adapted functions $X_{lh}^{p\mu}$ [31]. The cut-off parameters used in these expansions were $l_c = 30$ and $h_c = 30$ for all bound and continuum orbitals, whereas the T-matrix elements were truncated at $l_c = 28$ and $h_c = 28$ for energies up to 50 eV and at $l_c = 30$ and $h_c = 30$ for higher energies. The calculated cross sections were converged up to 10 iterations.

Also, a Born-closure formula was used to account for the contribution of higher partial-wave components of the scattering amplitudes. This procedure, used in some of our previous studies [12, 32, 33], is necessary due to the slow convergence of T-matrix partial-wave expansion for polar targets.

IV. RESULTS AND DISCUSSION

A. Methyl Formate

Our experimental DCS, ICS, and MTCS for elastic electron scattering by methyl formate in the 30–800 eV range are listed in Table I. The extrapolated DCS at regions not covered in the experiment were also included. In general, they were obtained following the trend of the MCOP calculations. Nonetheless, for energies higher than 150 eV and angles larger than 120°, the extrapolated DCS were obtained following the trend of the IAM. Comparisons of present experimental DCS with calculated results using the MCOP are shown in Figs. 1–3, along with our results calculated using the IAM as described in Ref. [9]. In general, the MCOP DCS agree well with the present measured results. Nevertheless, at 300 eV and above, the MCOP results underestimate the DCS at large scattering angles. This discrepancy was also observed in our recent electron-acetone scattering study [14]. It is mainly due to the lack of convergence in the single-center expansion of the nuclear part of U_{st} for atoms a few angstroms away from the expansion center. The effects of this lack of convergence are particularly enhanced at high incident energies due to the fact that the scattering electron may penetrate more deeply into the target.

At 150 eV and below, the IAM calculations clearly overestimate the experimental DCS. Nevertheless such discrepancies decrease with increasing incident energies. It is interesting

to note that, for energies higher than 300 eV and large scattering angles, the theoretical results calculated using the IAM are in better agreement with the measured data than those of MCOP. This is due to the multicentric nature of the interaction potential used in IAM calculations [34].

In Fig. 4, we present our theoretical ICS and MTCS calculated using the MCOP for electron scattering by methyl formate in the 1–500 eV range. The present experimental results of ICS and MTCS in the 30–500 eV range are also shown for comparison. There is a very good agreement between our calculated and measured data in this energy range. Unfortunately, at energies below 30 eV, no other results of ICS and MTCS for this target are available in the literature. However, a theoretical investigation on electron scattering by acetic acid at energies up to 10 eV was published by Freitas *et al.* [35]. Since methyl formate and acetic acid are isomers, a comparison of their ICS calculated using the SMC at static-exchange (SE) and static-exchange-polarization (SEP) levels of approximations [35] with our data may provide some interesting information. In this low energy region, both our MCOP ICS and MTCS show two structures: one peak located at incident energies around 3.0 eV and a broad resonance-like feature centered at about 8 eV. The partial-channel cross section analysis showed that the first peak is due to a strong $^2A''$ resonance located at 3.0±0.1 eV with a width of 0.8 eV. This resonance is well known in electron scattering experiments with targets containing a carbonyl group. In such systems, the empty π^* orbital of that group may trap a low-energy scattering electron to form a metastable ion and thus supports a shape resonance [14, 21, 38]. This resonance was also identified in the $^2A''$ scattering channel in electron – acetic acid study of Freitas *et al.* [35], located at about 4.2 eV in their SE and 1.8 eV in the SEP calculations. Moreover, the resonance located at about 8.0 eV seen in the present study was identified to have a $^2A'$ symmetry. This resonance also occurs in electron scattering by hydrocarbons [19, 20] and is of a $k\sigma^*$ nature, as already discussed by Kimura *et al.* [39]. In contrast, Freitas *et al.* found two structures in the $^2A'$ scattering channel, including one located at around 8 eV. However, both structures were considered spurious and therefore disregarded by the authors.

In Fig. 5(a), we present our theoretical TCS for electron scattering by methyl formate in the 1–500 eV range. Unfortunately, there are neither theoretical nor experimental results of TCS reported for this target to compare with our data. In Fig. 5(b), the present TACS are compared with experimental TICS of Hudson *et al.* [6] at incident energies from near

threshold to 285 eV. In general, there is a very good qualitative agreement between our calculated TACS and experimental TICS. Quantitatively, there is also a very good agreement for energies above 100 eV. At lower energies, our TACS lie in general above the TICS. This is due to the fact that TACS account for both excitation and ionization channels, while the measured TICS do not include excitation processes. Near threshold, the experimental TICS are larger than our TACS, which may be due to the unstability of the trap current regulation below 15 eV, as stated by the authors [6].

For completeness, our MCOP DCS in the 1–20 eV range are shown in Suplemental Material [36].

B. Ethyl Acetate

For this molecule, the MCOP calculations would be too involved and therefore comparisons are made only with our theoretical results calculated using the IAM. They are shown in Figs. 6–8. In general, our calculated IAM DCS agree qualitatively well with the present measured results. As expected, the IAM calculations clearly overestimate the experimental DCS at 100 eV and below. Even at energies as high as 500 eV, the IAM still strongly overestimates the experimental DCS at small scattering angles. Also, as seen for methyl formate, the discrepancies between experiment and the IAM diminish with increasing incident energies.

In Fig. 9 we compare our experimental ICS and MTCS measured at 30–1000 eV range with those calculated using the IAM. Present theoretical results obtained using the additivity rule (AR) [40] are also shown. Our IAM calculations strongly overestimate the experimental ICS. This is directly related to the small-angle behavior of the IAM DCS as stated above. On the other hand, the present AR ICS are in reasonably good agreement with our measured data.

In a recent study, Blanco and García [41] investigated the relevance of the interference terms in the IAM. In that study, they calculated DCS and ICS for both electron and positron scattering by two small targets, namely H_2 and CH_4, in the 30–300 eV range. A numerical integration of the Lippmann-Schwinger equation over a three dimensional multicentric potential was used. The comparison of these calculated cross sections with those obtained using the IAM and AR showed that the interference effects are not negligible at the interme-

diate and high energies. Nevertheless, for a number of molecules, the comparison between the experimental ICS with those obtained using the IAM has systematically shown poorer agreement than those of AR [9, 42]. An possible explanation is as follows. In IAM calculations, the e^-–molecule interaction is represented simply by a sum of atomic potentials. Certainly, such approximation would fail at low incident energies, where the projectile electron has less penetration power into the molecule and so the scattering would be dominated by long-range potentials. Next, the IAM in its usual form does not include intramolecular multiple-scattering effects (IMSE). The relevance of such effects was investigated by Iga *et al.* [43] in 1999 for electron scattering by N_2 in the 50–1000 eV range. The authors showed that even at 300 eV, the IMSE reduce significantly the DCS at small scattering angles. In addition, it is also expected that the IMSE would be more relevant with increasing molecular size (number and weight of atoms). The inclusion of IMSE in calculations would significantly improve the agreement between the IAM DCS and experimental results at small scattering angles. In this sense, the better agreement between experimental and AR ICS may be fortuitous due to the absence of both IMSE and interference terms which leads to opposite contributions to ICS. On the other hand, the IAM MTCS agree fairly well with both the AR and experimental MTCS, probably because the contributions of the small-angle DCS to the MTCS are less important.

For completeness, the experimental DCS, ICS, and MTCS in the 30–1000 eV range are listed in Table II. For this system, extrapolated DCS in the angular range not covered in the experiment were also included. At small angles, they were obtained visually and at large angles they followed the trend of the IAM calculations;

V. CONCLUSIONS

This study reports an experimental investigation on elastic electron collisions with two small esters, methyl formate and ethyl acetate, in a wide energy range. More precisely, absolute DCS, ICS, and MTCS for these targets were measured in the 30–1000 eV range. The present study is mainly motivated by the lack of experimental cross sections for these targets in the literature. Particularly, for methyl formate, a theoretical investigation based on the MCOP interaction combined with the Padé approximation was also carried out. Our measured data for methyl formate are in generally good agreement with our theoretical

data calculated using the MCOP model. We have also identified a sharp resonance in the $^2A''$ scattering channel at about 3.0 eV. This π^*-type resonance is well known in electron scattering experiments with targets containing a carbonyl group [14, 21, 38]. In addition, a σ^*-type resonance centered at about 8.0 eV is identified in the $^2A''$ scattering channel.

For ethyl acetate, the comparison of our experimental results is made only with those calculated using the IAM and the AR. Despite a very good qualitative agreement, the IAM calculations overestimate the experimental DCS at energies of 100 eV and below.

ACKNOWLEDGMENTS

The authors would like to thank G. H. Davanzo and G. E. O. Camargo for their valuable help. This research was partially supported by the agencies CNPq(Brazil), FAPESP(Brazil) and CAPES(Brazil).

[1] G. W. Huber, S. Iborra, and A. Corma, Chem. Rev. **107** 4044 (2006).

[2] A. Remijam, Y.-S. Shiao, D. N. Friedel, D. S. Meier, L. E. Snyder, ApJ. **617**, 384 (2004).

[3] S. Liu, D. M. Mehringer, and L. E. Snyder, ApJ. **552**, 654 (2001).

[4] S. Cradock and D. H. Rankim, J. Mol. Struct. **69**, 145 (1980).

[5] I. Ishii and A. P. Hitchcock, J. Electon Spectr. Rel. Phenom. **46**, 55 (1988).

[6] J. E. Hudson, Z. F. Weng, C. Vallance, and P. W. Harland, Int. J. Mass Spectr. **248**, 42 (2006).

[7] I. Iga, M. T. Lee, M. G. P. Homem, L. E. Machado, and L. M. Brescansin, Phys. Rev. A **61**, 022708 (2000).

[8] P. Rawat, I. Iga, M. T. Lee, L. M. Brescansin, M. G. P. Homem, and L. E. Machado, Phys. Rev. A **68**, 052711 (2003).

[9] M. G. P. Homem, R. T. Sugohara, I. P. Sanches, M. T. Lee, and I. Iga, Phys. Rev. A **80**, 032705 (2009).

[10] M. G. P. Homem, I. Iga, R. T. Sugohara, I. P. Sanches, and M. T. Lee, Rev. Sci. Instrum. **82**, 013109 (2011).

[11] R. T. Sugohara, M. G. P. Homem, I. P. Sanches, A. F. de Moura, M. T. Lee, and I. Iga, Phys. Rev. A **83**, 032708 (2011).

[12] M.-T. Lee, G. L. C. de Souza, L. E. Machado, L. M. Brescansin, A. S. dos Santos, R. R. Lucchese, R. T. Sugohara, M. G. P. Homem, I. P. Sanches, and I. Iga, J. Chem. Phys. **136**, 114311 (2012).

[13] R. T. Sugohara, M. G. P. Homem, G. L. C. de Souza, L. E. Machado, J. R. Ferraz, A. S. dos Santos, L. M. Brescansin, R. R. Lucchese, and M.-T. Lee, Phys. Rev. A **88**, 022709 (2013).

[14] M. G. P. Homem, I. Iga, L. A. da Silva, J. R. Ferraz, L. E. Machado, G. L. C. de Souza, V. A. S. da Mata, L. M. Brescansin, R. R. Lucchese, and M.-T. Lee, Phys. Rev. A **92**, 032711 (2015).

[15] S. K. Srivastava, A. Chutjian and S. Trajmar, J. Chem. Phys. **63**, 2659 (1975).

[16] T. W. Shyn and G. R. Carignan, Phys. Rev. A **22**, 923 (1980).

[17] R. H. J. Jansen, F. J. de Heer, H. J. Luyken, B. van Wingerden, and H. J. Blaauw, J. Phys. B **9**, 185 (1976).

[18] R. D. DuBois and M. E. Rudd, J. Phys. B **9**, 2657 (1976).

[19] P. Rawat, M. G. P. Homem, R. T. Sugohara, I. P. Sanches, I. Iga, G. L. C. de Souza, A. S. dos Santos, R. R. Lucchese, L. E. Machado, L. M. Brescansin, and M.-T. Lee, J. Phys. B **43**, 225202 (2010).

[20] G. L. C. de Souza, M.-T. Lee, I. Iga, I. P. Sanches, P. Rawat, I. Iga, A. S. dos Santos, L. E. Machado, R. T. Sugohara, L. M. Brescansin, M. G. P. Homem, and R. R. Lucchese, Phys. Rev. A **82**, 012709 (2010).

[21] J. R. Ferraz, A. S. dos Santos, G. L. C. de Souza, A. I. Zanelato, T. R. M. Alves, M.-T. Lee, L. M. Brescansin, R. R. Lucchese, and L. E. Machado, Phys. Rev. A **87**, 032717 (2013).

[22] F. A. Gianturco, R. R. Lucchese, and N. Sanna, J. Chem. Phys. **102**, 5743 (1995).

[23] A. R. Edmonds, *Angular Momentum and Quantum Mechanics* Princeton University Press, Princeton, NJ (1960).

[24] N. T. Padial and D. W. Norcross, Phys. Rev. A **29**, 1742 (1984).

[25] M.-T. Lee, I. Iga, L. E. Machado, L. M. Brescansin, E. A. y Castro, I. P. Sanches, and G. L. C. de Souza, J. Electron Spectrosc. Relat. Phenom. **155**, 14 (2007).

[26] E. A. y Castro, G. L. C. de Souza, I. Iga, L. E. Machado, L. M. Brescansin, and M.-T. Lee, J. Electron Spectrosc. Relat. Phenom. **159**, 30 (2007).

[27] G. Staszewska, D. W. Schwenke, and D. G. Truhlar, Phys. Rev. A **29**, 3078 (1984).

[28] S. Hara, J. Phys. Soc. Japan **22**, 710 (1967).

[29] M. W. Schmidt, K. K. Baldridge, J. A. Boatz, S. T. Elbert, M. S. Gordon, J. H. Jensen, S. Koseki, N. Matsunaga, K. A. Nguyen, S. Su, T. L. Windus, M. Dupuis, and J. A. Montgomery, J. Comput. Chem. **14**, 1347 (1993).

[30] http://cccbdb.nist.gov

[31] P. G. Burke, N. Chandra, and F. A. Gianturco, J. Phys. B **5**, 2212 (1972).

[32] L. M. Brescansin, L. E. Machado, M.-T. Lee, H. Cho, and Y. S. Park, J. Phys. B **41**, 185201 (2008).

[33] L. E. Machado, L. M. Brescansin, I. Iga, and M.-T. Lee, Eur. Phys. **33**, 193 (2005).

[34] M.-T. Lee and L. C. G. Freitas, J. Phys. B **13**, 233 (1983).

[35] T. C. Freitas, M. T. do N. Varella, R. F. da Costa, M. A. P. Lima, and M. H. F. Bettega, Phys. Rev A **79**, 022706 (2009).

[36] See Supplemental Material at [URL will be inserted by publisher].

[37] M. A. Khakoo, J. Blumer, K. Keane, C. Campbell, H. Silva, M. C. A. Lopes, C. Winstead, V. McKoy, R. F. da Costa, L. G. Ferreira, M. A. P. Lima, and M. H. F. Bettega, Phys. Rev A **77**, 042705 (2008).

[38] M. G. P. Homem, I. Iga, G. L. C. de Souza, A. I. Zanelato, L. E. Machado, J. R. Ferraz, A. S. dos Santos, L. M. Brescansin, R. R. Lucchese, and M.-T.Lee, Phys. Rev. A **90**, 062704 (2014).

[39] M. Kimura, O. Sueoka, A. Hamada, and Y. Itikawa, Adv. Chem. Phys. **111**, 537 (2000).

[40] D. Shi, J. Sun, Y. Liu, and Z. Zhu, J. Phys. B **41**, 025205 (2008).

[41] F. Blanco and G. García, Chem. Phys. Lett. **635**, 321 (2015).

[42] I. P. Sanches, R. T. Sugohara, L. Rosani, M.-T.Lee,and I. Iga, J. Phys. B **41**, 185202 (2008).

[43] I. Iga, R. A. Bonham, and M.-T.Lee, J. Mol. Struct. **468**, 241 (1999).

TABLE I. Experimental DCS (in 10^{-16} cm^2/sr), ICS and MTCS (in 10^{-16} cm^2) for elastic e$^-$-methyl formate scattering. Extrapolated values are given in parentheses.

Angle	E(eV)								
(deg)	30	50	100	150	200	300	400	500	800
3	(53)	(65)	(75)	(95)	(80)	(78)	(75)	(70)	(60)
5	(51)	(60)	(68)	(71)	(65)	(57)	(56)	(49)	(30)
10	(40)	40.83	26.56	13.84	11.14	11.72	7.39	7.89	3.20
15	23.93	19.56	10.49	4.92	3.76	2.93	2.49	2.62	1.45
20	14.77	8.90	3.04	2.50	1.99	1.42	1.24	1.27	0.875
25	6.73	(3.97)	1.68	1.55	1.19	0.775	0.710	0.907	0.549
30	3.91	1.97	1.03	0.997	0.723	0.549	0.574	0.635	0.283
35	(2.57)	(1.39)	0.739	0.559	(0.54)	0.434	0.398	0.349	(0.19)
40	1.71	0.957	0.519	0.370	0.427	0.319	0.230	0.207	0.121
50	0.958	0.657	0.299	0.261	0.275	0.160	0.123	0.119	0.058
60	0.757	0.437	0.226	0.166	0.158	0.098	0.086	0.081	0.034
70	0.532	0.272	0.156	0.095	0.115	0.083	0.061	0.052	0.024
80	0.431	0.209	0.137	0.083	0.101	0.065	0.043	0.040	0.016
90	0.347	0.189	0.109	0.096	0.093	0.055	0.037	0.034	0.011
100	0.366	0.199	0.109	0.099	0.096	0.055	0.033	0.029	0.009
110	0.440	0.268	0.125	0.101	0.091	0.053	0.031	0.026	0.008
120	0.680	0.358	0.170	0.119	0.087	0.049	0.030	0.024	0.007
130	(0.91)	(0.55)	0.212	0.120	(0.09)	(0.05)	(0.03)	(0.02)	0.006
140	(1.16)	(0.68)	(0.23)	(0.12)	(0.10)	(0.05)	(0.03)	(0.02)	(0.006)
150	(1.44)	(0.83)	(0.27)	(0.12)	(0.11)	(0.05)	(0.03)	(0.02)	(0.006)
160	(1.76)	(0.97)	(0.31)	(0.13)	(0.12)	(0.05)	(0.03)	(0.02)	(0.006)
170	(1.98)	(1.10)	(0.36)	(0.13)	(0.12)	(0.05)	(0.03)	(0.02)	(0.006)
180	(2.19)	(1.16)	(0.38)	(0.14)	(0.12)	(0.05)	(0.03)	(0.02)	(0.006)
ICS	24.6	18.1	11.1	8.5	7.4	6.2	5.3	5.0	3.0
MTCS	11.0	6.3	2.6	1.6	1.5	0.87	0.60	0.52	0.21

TABLE II. Experimental DCS (in 10^{-16} cm^2/sr), ICS and MTCS (in 10^{-16} cm^2) for elastic e$^-$-ethyl acetate scattering. Extrapolated values are given in parentheses.

Angle	E(eV)									
(deg)	30	50	100	150	200	300	400	500	800	1000
3	(123)	(180)	(175)	(110)	(90)	(85)	(80)	(75)	(67)	(47)
5	(111)	(160)	(150)	(90)	71.41	66.22	60.65	40.60	(45)	24.39
10	(70)	(77)	37.87	46.79	18.50	13.24	10.34	7.30	6.43	5.03
15	34.17	25.03	11.74	12.46	6.06	4.33	4.37	3.68	2.02	1.89
20	13.73	12.10	3.77	4.57	3.42	2.99	2.29	1.55	1.36	1.39
25	7.43	5.72	1.87	2.49	2.32	1.46	1.27	1.11	0.788	0.590
30	4.58	3.22	1.27	1.49	1.24	1.05	1.02	0.851	0.381	0.316
40	2.14	1.57	0.812	0.604	0.634	0.593	0.379	0.260	0.177	0.132
50	0.968	1.31	0.457	0.379	0.418	0.248	0.199	0.156	0.084	0.062
60	0.789	0.624	0.340	0.233	0.217	0.183	0.130	0.099	0.047	0.036
70	0.478	0.478	0.252	0.145	0.183	0.135	0.085	0.062	0.032	0.022
80	0.439	0.294	0.151	0.151	0.178	0.097	0.064	0.046	0.022	0.015
90	0.497	0.223	0.138	0.145	0.139	0.078	0.055	0.035	0.014	0.011
100	0.538	0.237	0.144	0.134	0.135	0.074	0.048	0.029	0.012	0.008
110	0.635	0.318	0.179	0.160	0.117	0.067	0.040	0.025	0.010	0.007
120	1.02	0.424	0.207	0.167	0.122	0.066	0.039	0.022	0.008	0.006
130	(1.72)	(0.67)	(0.25)	(0.18)	(0.14)	(0.07)	(0.04)	(0.02)	(0.008)	(0.006)
140	(2.65)	(0.89)	(0.30)	(0.19)	(0.16)	(0.07)	(0.03)	(0.02)	(0.007)	(0.005)
150	(3.64)	(1.12)	(0.35)	(0.21)	(0.17)	(0.07)	(0.03)	(0.02)	(0.007)	(0.005)
160	(4.50)	(1.33)	(0.39)	(0.23)	(0.17)	(0.07)	(0.03)	(0.02)	(0.006)	(0.004)
170	(5.05)	(1.47)	(0.43)	(0.24)	(0.18)	(0.07)	(0.03)	(0.02)	(0.006)	(0.004)
180	(5.25)	(1.52)	(0.44)	(0.25)	(0.18)	(0.07)	(0.03)	(0.02)	(0.006)	(0.004)
ICS	37.9	31.1	17.7	15.3	10.3	8.1	6.9	5.2	4.3	2.9
MTCS	20.7	8.5	3.4	2.6	2.2	1.3	0.84	0.58	0.29	0.22

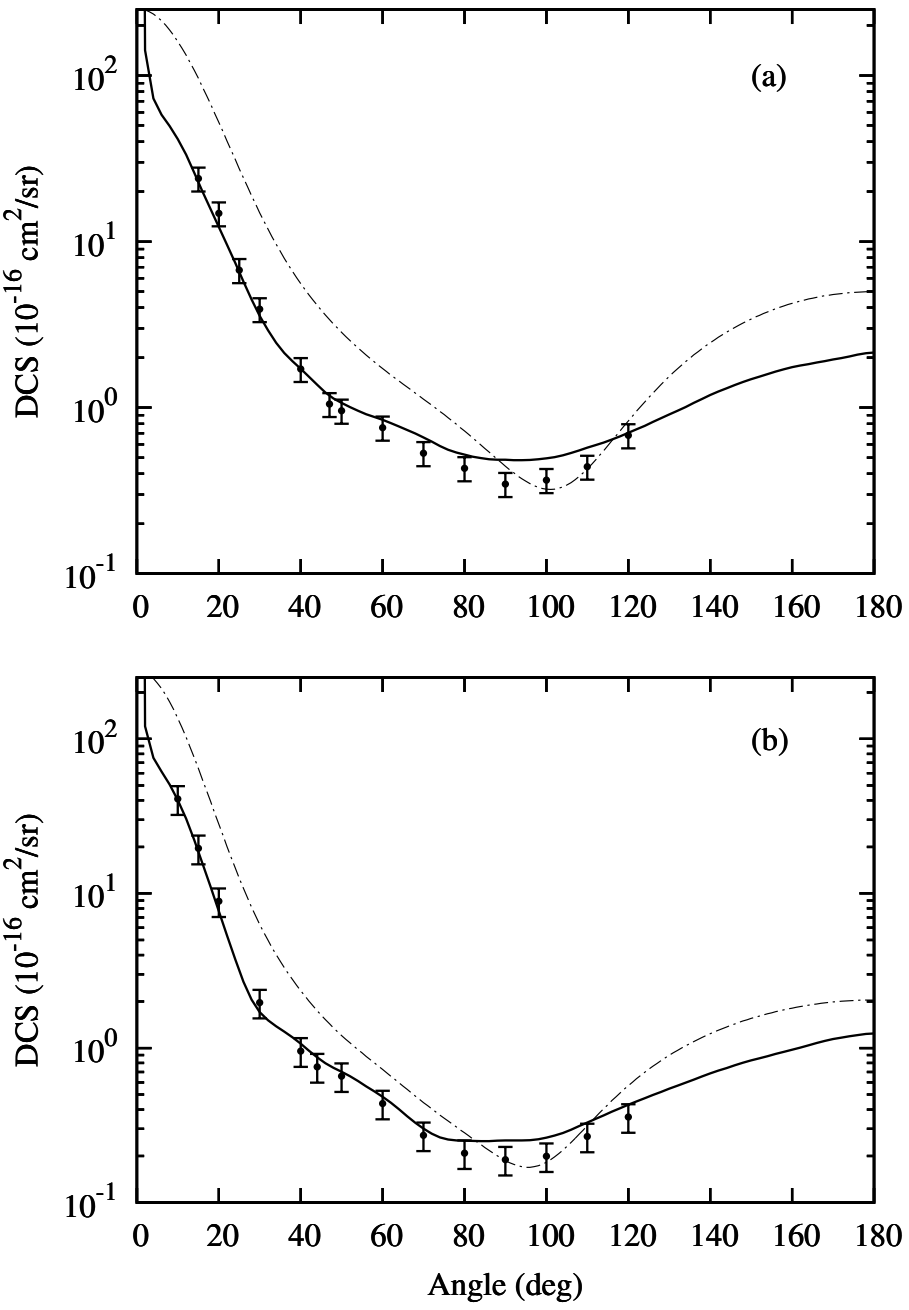

FIG. 1. DCS for elastic e^-–methyl formate scattering at (a) 30 eV and (b) 50 eV. Full curve, present MCOP results; dash-dotted curve, present IAM results; full circles, present experimental results.

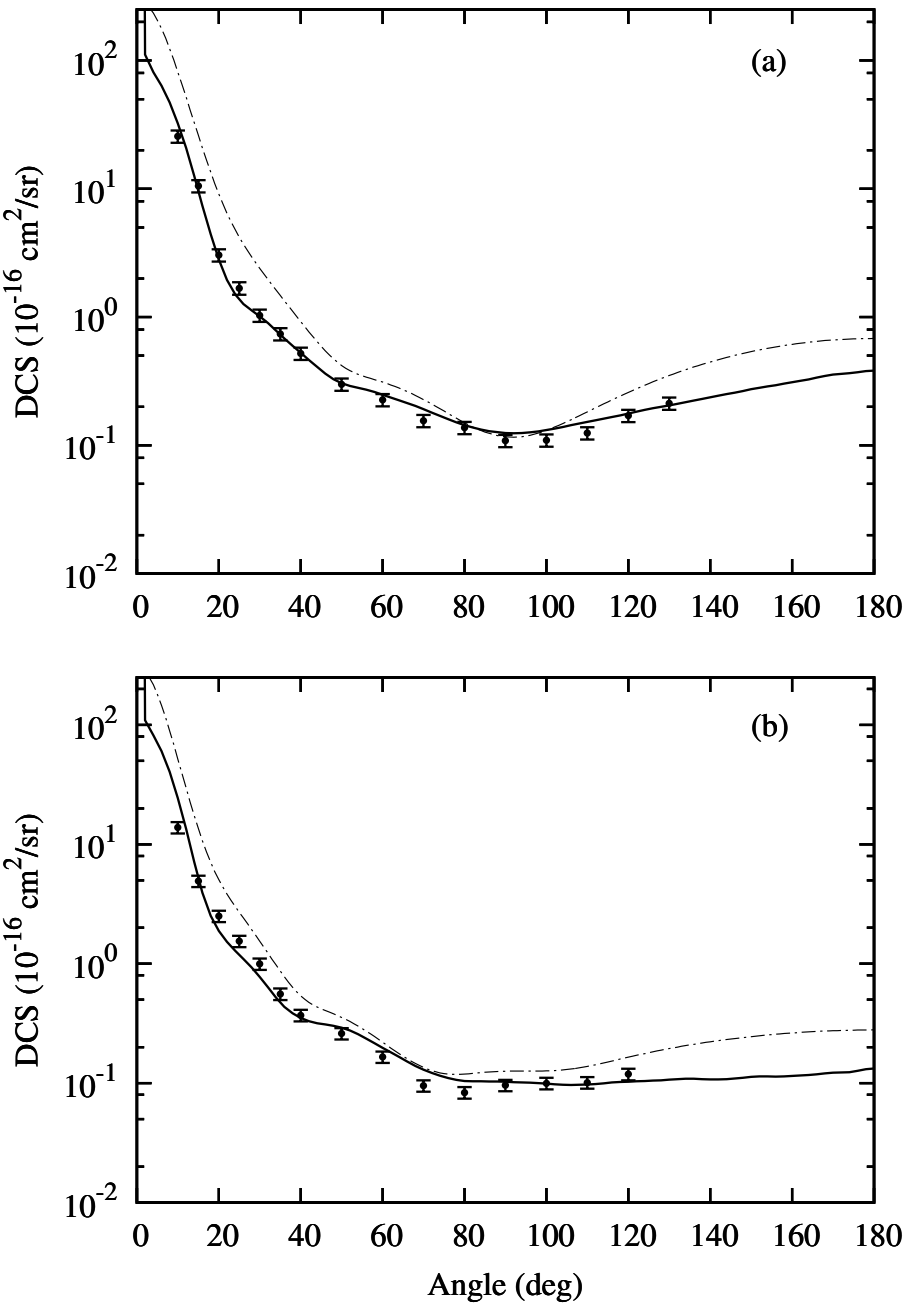

FIG. 2. Same as in Fig. 1 but at (a) 100 eV and (b) 150 eV.

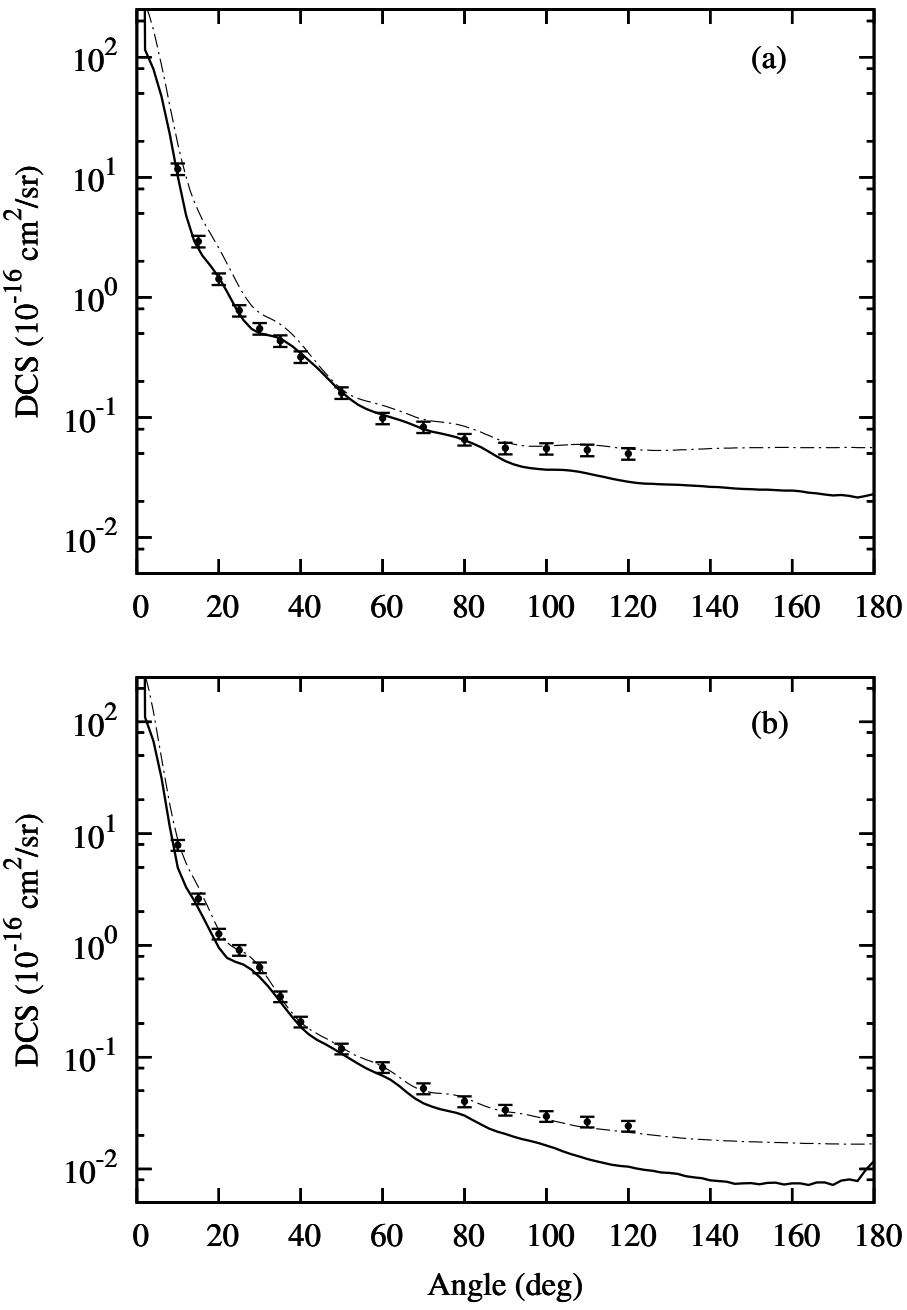

FIG. 3. Same as in Fig. 1 but at (a) 300 eV and (b) 500 eV.

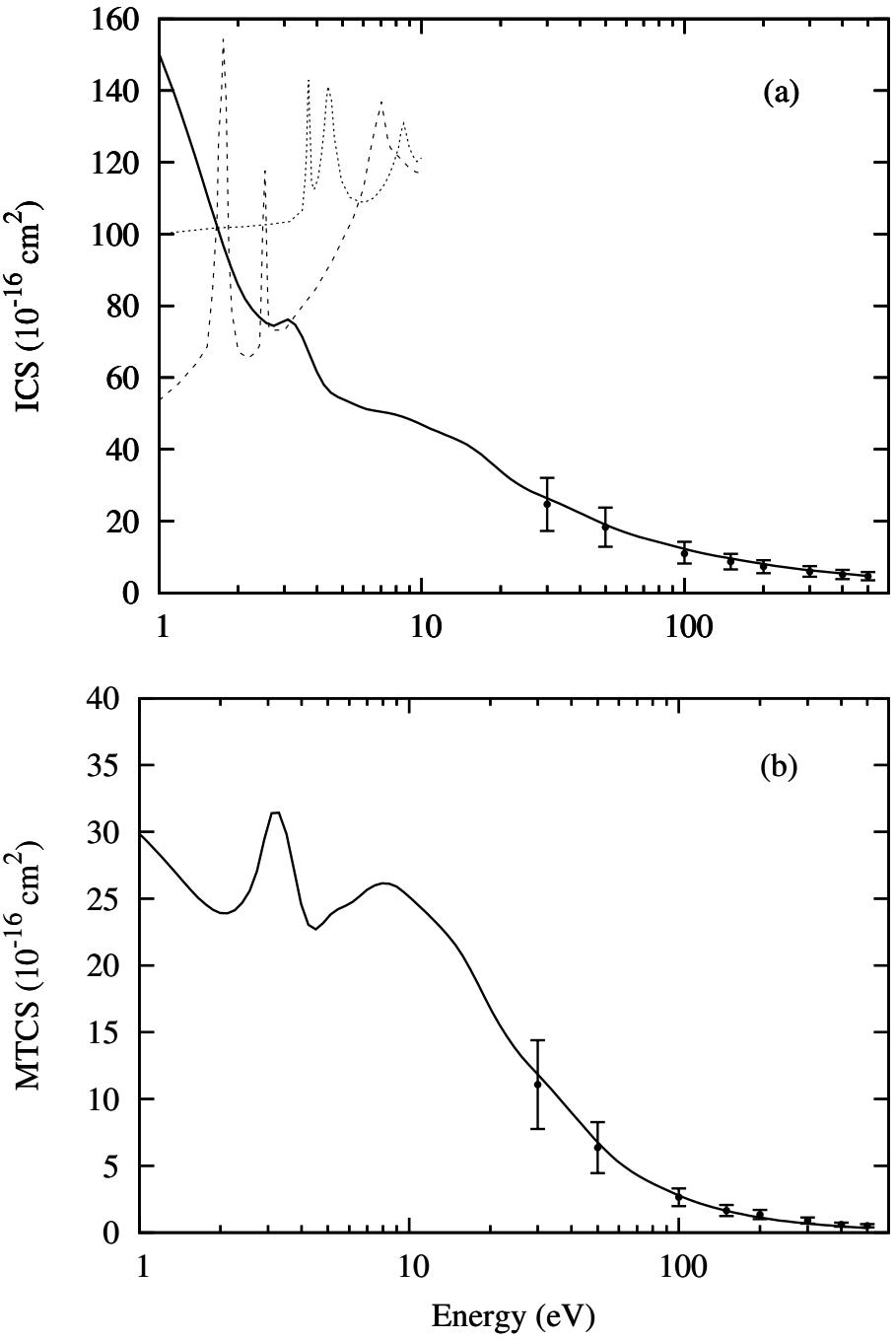

FIG. 4. (a) ICS and (b) MTCS for elastic e^-–methyl formate scattering. Full curve, present calculated data using the MCOP; dashed curve, SMC SEP ICS; short-dashed curve, SMC SE ICS, both for e^-–acetic acid scattering of Freitas *et al.* [35]; full circles, present experimental data.

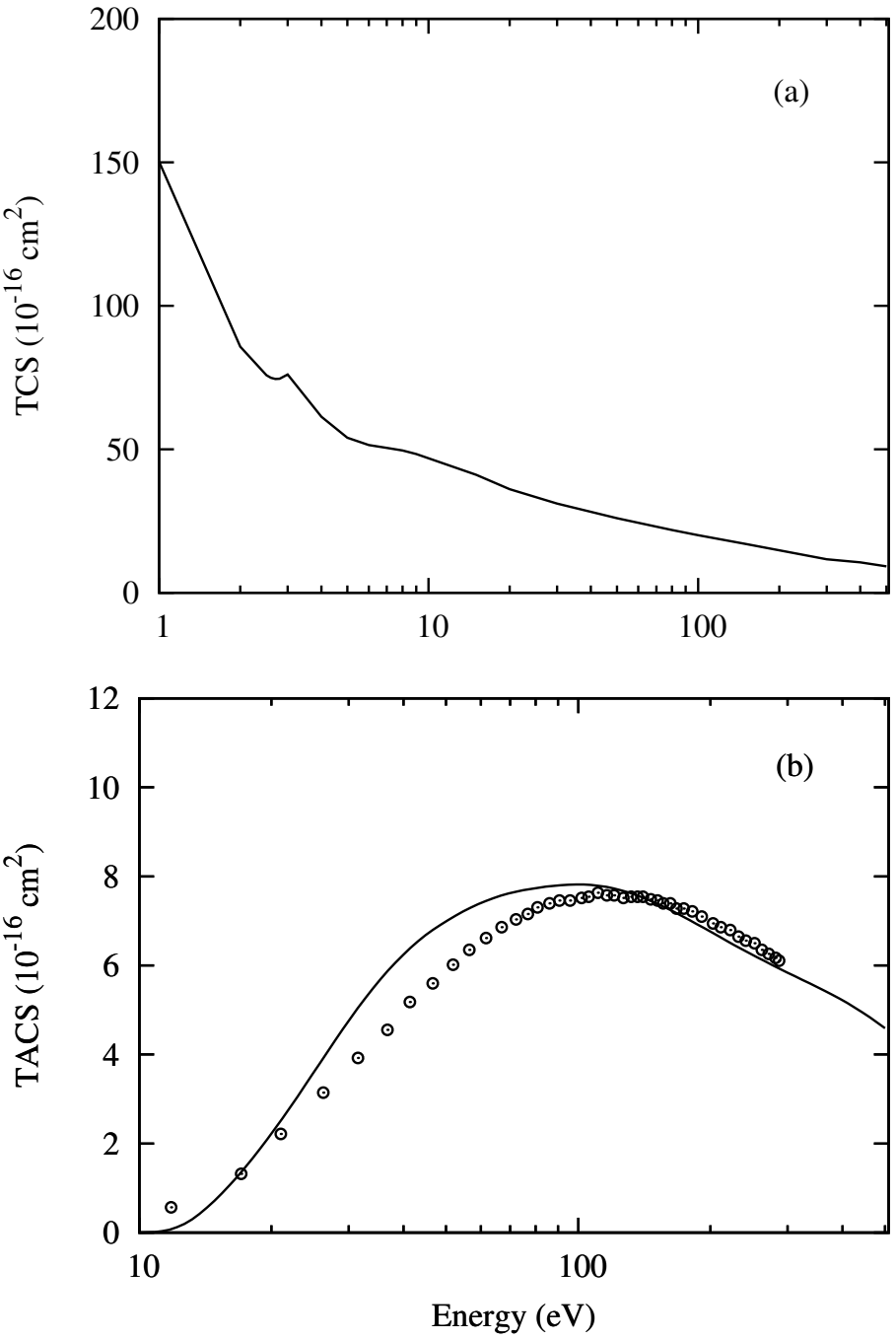

FIG. 5. (a) TCS and (b) TACS for e^-–methyl formate scattering. Full curve, present data calculated using the MCOP; open circles, experimental TICS of Hudson *et al.* [6].

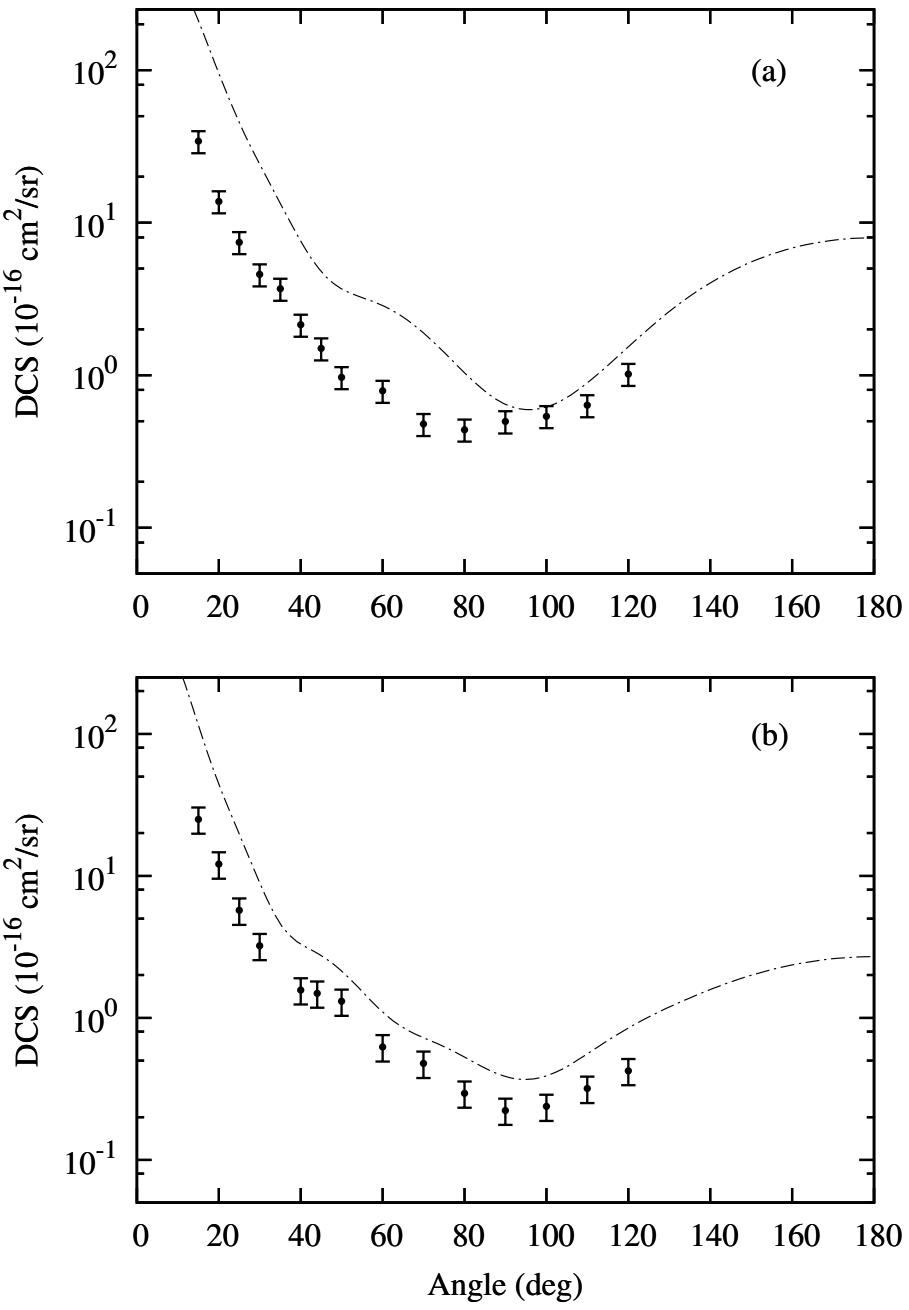

FIG. 6. DCS for elastic e^-–ethyl acetate scattering at (a) 30 eV and (b) 50 eV. Dash-dotted curve, present IAM results; full circles, present experimental results.

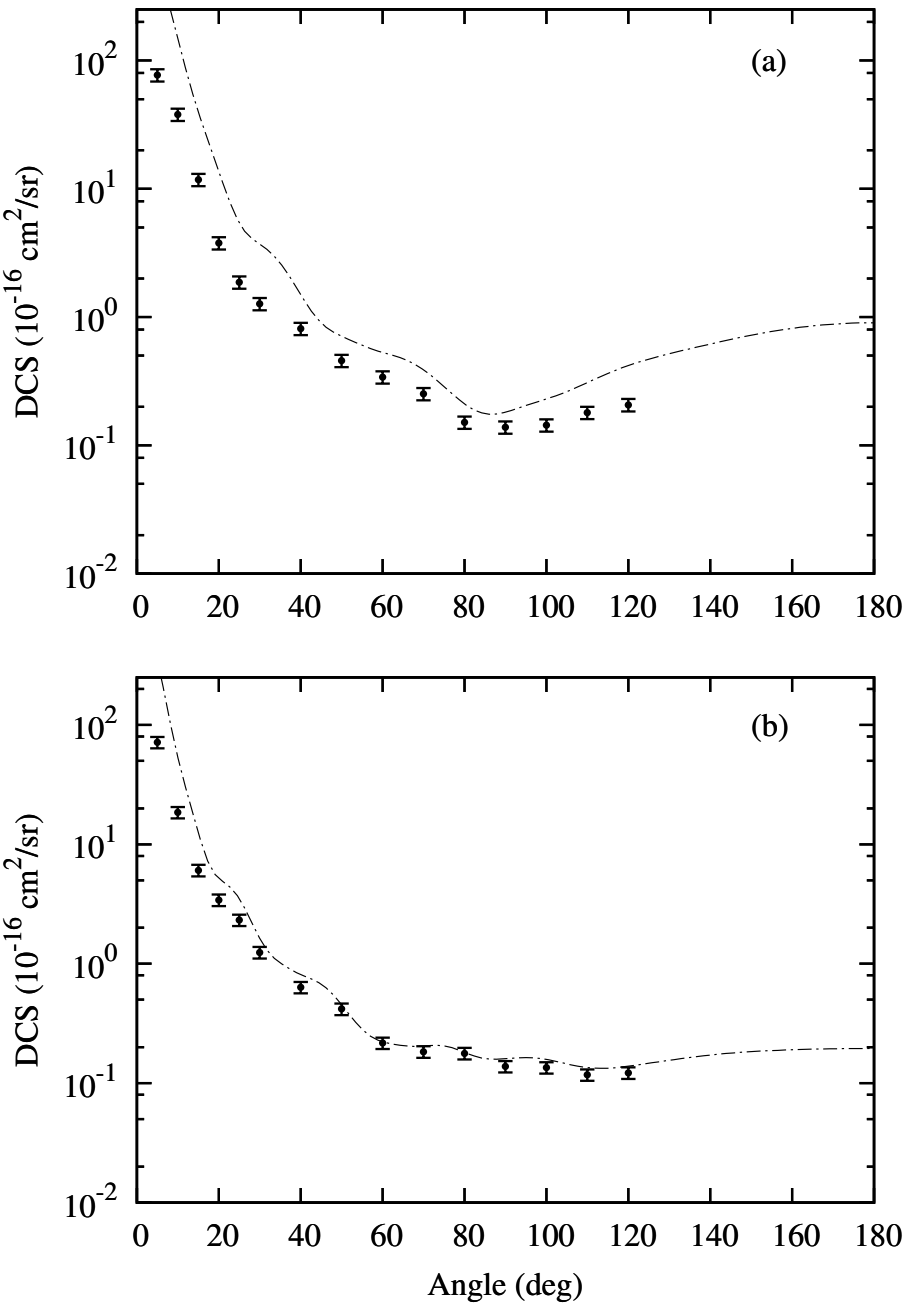

FIG. 7. Same as in Fig. 6 but at (a) 100 eV and (b) 200 eV.

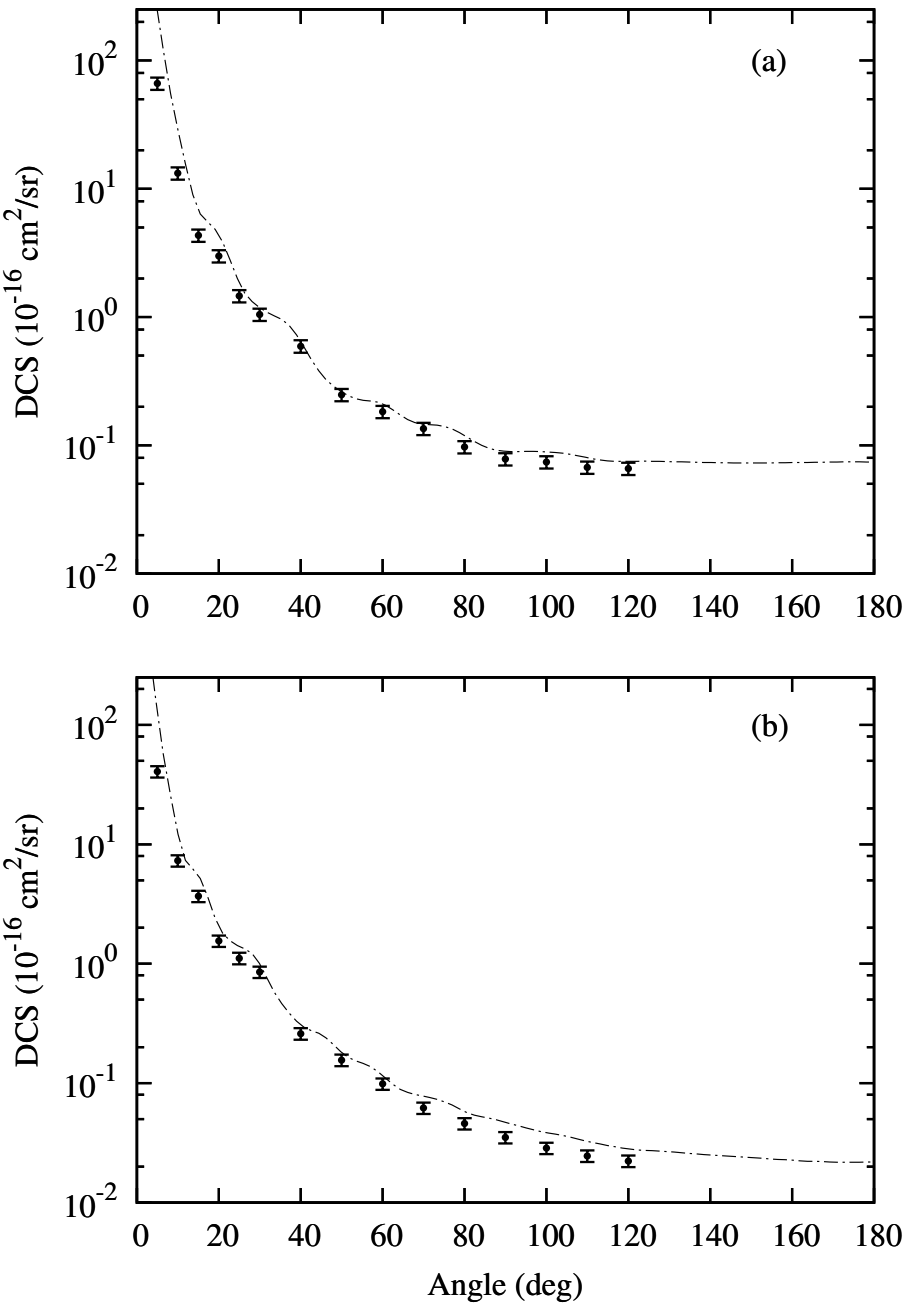

FIG. 8. Same as in Fig. 6 but at (a) 300 eV and (b) 500 eV.

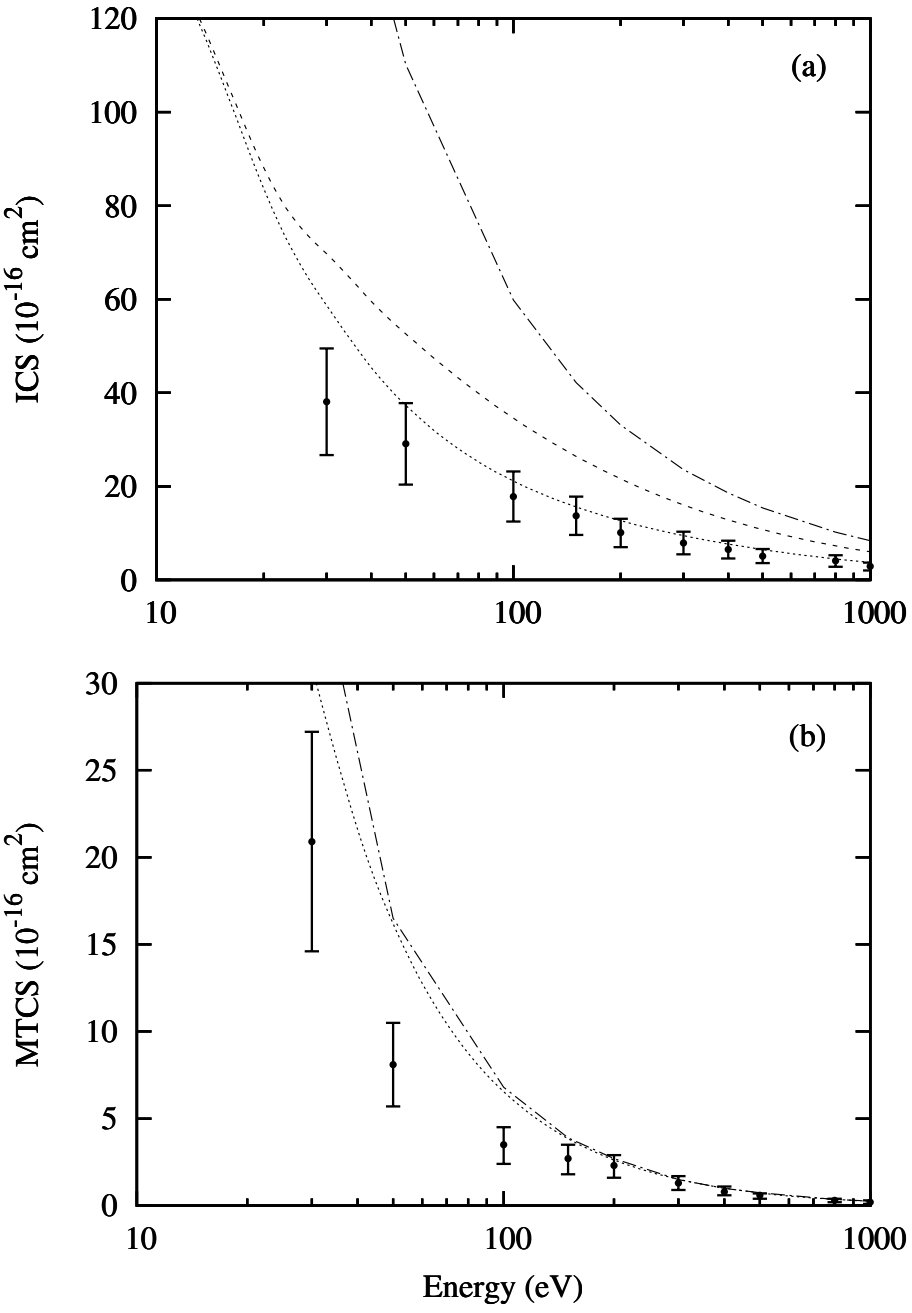

FIG. 9. (a) ICS and (b) MTCS for elastic e^-–ethyl acetate scattering. Dash-dotted curve, present calculated data using the IAM; dotted curve, present calculated data using the AR; dashed curve, present TCS data calculated using the AR; full circles, present experimental data.